Metal hydroxide salt monolayer nanoparticles: synthesis, redox characterization, and electrochemical catalytic performance

Naoki Tarutani* †‡, Sota Kimura†, Takuya Sakata†§, Kazumasa Suzuki#, Kiyofumi Katagiri†, and Kei Inumaru†

† Graduate School of Advanced Science and Engineering, Hiroshima University, Higashi-Hiroshima 739-8527, Japan.

‡ CAT Fellow, Institute for Catalysis, Hokkaido University, Sapporo 001-0021, Japan.

§ Western Region Industrial Research Center, Hiroshima Prefectural Technology Research Institute, 2-10-1 Aga-Minami, Kure 737-0004, Japan

Department of Materials Science, The University of Shiga Prefecture, Hikone, Shiga 522-8533, Japan

ABSTRACT: Two-dimensional materials modified with low molecules are known to show unique electronic properties. In this study, we focus on the synthesis and electrochemical investigation of metal hydroxide salt monolayer nanoparticles modified with different molecules towards improved electrochemical functions. Nickel hydroxide carboxylate nanoparticles are successfully prepared through the epoxide-mediated alkalinization method using alkylcarboxylates. It is found that the monolayer nanoparticles with a size of approximately 2 nm are formed directly from an ionic precursor or after ultrasonication post-treatment. Manganese, iron, and cobalt hydroxide carbonates are found to form monolayer nanoparticles through the same procedure. Synthetic nickel hydroxide carbonate monolayer nanoparticles with a short alkylcarboxylate show enhanced redox process and electrochemical functions owing to high proton diffusion coefficient, lowered electron transfer resistance and improved intrinsic catalytic activity. We propose that the results obtained in this study will provide a novel design strategy for metal hydroxide monolayer nanoparticulate catalysts towards high functionality.

Since the discovery of graphene, the design of materials using two-dimensional substances has attracted much attention.[1] For example, assembled mesostructures,[2,3] hetero-stacking structures, such as graphene/hBN[4] and MoS_2/graphene,[5] and aligned hetero-growth in the lateral direction, such as graphene/MoS_2,[6] WS_2/MoS_2[7] and halide perovskite,[8] have been synthesized and used as novel electronic devices. Furthermore, surface modification of two-dimensional materials by using low molecule species was found to enable tuning of the physical properties.[9] These designs of two-dimensional-based materials have been started to investigate widely.[10]

The layered metal hydroxide family, including layered double hydroxides, layered rare-earth hydroxides and layered hydroxide salts, is known to delaminate and form two-dimensional nanosheets.[11–13] Different from van der Waals two-dimensional materials, such as graphene and metal chalcogenides, a two-dimensional layer of a metal hydroxide has a positive charge. This feature enables the intercalation and exchange of anionic ions including organic molecules. Intercalation of large anions, such as dodecyl sulphate,[14] and/or using a polar solvent[11] enable a weakening of the interaction among layers and the formation of delaminated monolayers. Delaminated hydroxide monolayers are reported to show unique properties, such as anisotropic hydroxyl ion conduction.[15] Much attention has focused on their use as an electrochemical catalyst for the oxygen evolution reaction of water splitting. Layered double hydroxides have shown extraordinarily high catalytic performance by delaminating their layered structure.[16] Reduction of the size in the lateral direction during delamination is expected to increase number of dangling bonds and contribute to the catalytic activity. In addition, the suggested catalytic mechanism of metal hydroxide on the oxygen evolution reaction includes the interaction of water molecules and a surface ligand;[17,18] therefore, the design of surface modifier molecules will be of high importance. Monolayer nanoparticles of metal hydroxides have been synthesized and used as electrochemical catalysts. The top-down approach using ultrasonication was a successful route to synthesize single-nm-sized (< 3 nm) metal hydroxide monolayers,[19,20] which showed improved catalytic performances. However, surface-adsorbed formamide is mandatory to delaminate the layered structure, which inhibits the versatile modification of molecules towards electronic functionality tuning, as is shown in the MoS_2 monolayer case.[9] It is desirable to develop a novel synthetic pathway for metal hydroxide monolayer nanoparticles having single-nm-size modified with various functional molecules.

Bottom-up synthesis of monolayer hydroxides will allow tuning of the surface modifier molecules. Kuroda *et al*. reported a bottom-up synthesis of layered double hydroxide nanoparticles using a tripodal ligand modifier.[21]

Subsequent studies enabled a change of the modifier molecules and direct synthesis of sub-μm-sized monolayer metal hydroxides.[22,23] However, the control of the nanosheet size on the single-nm-scale with various modifier molecules has not yet been reported. Therefore, it is still difficult to tune both the size and chemical composition of metal hydroxide monolayer nanoparticles. In contrast, we found another methodology to synthesize single-nm-sized metal hydroxide nanoparticles using epoxide-mediated alkalinization.[24] Alkalinization process by using proton scavenge function of epoxides[25] accompanied by carboxylic acid coordination enabled the formation of single-nm-sized metal hydroxides.[26] This approach allowed a tuning of the size and cation composition of metal hydroxide nanoparticles.[27,28] Here, we first report the synthesis of manganese, iron, cobalt, and nickel hydroxide carboxylate monolayer nanoparticles through epoxide-mediated alkalinization and their redox and electrochemical performances (Figure 1). Nickel hydroxide carboxylate (NHC) nanoparticles modified with different lengths of alkylcarboxylate were employed to evaluate the effects of surface modifier molecules on the electrochemical properties. It was found that the NHC monolayer nanoparticles directly formed from the ionic precursor species in the case where a moderate length alkylcarboxylate was used (Figure 1a). An NHC with a short length of the alkyl chain enabled the redispersion in solvent and the formation of monolayer nanoparticles by ultrasonication post-treatment. However, NHC nanoparticles having long alkyl chain carboxylates became highly aggregated and were difficult to redisperse to form a monolayer shape. Infrared (IR) measurement, small angle X-ray scattering (SAXS), and transmission electron microscope (TEM) observation revealed that the monolayered nanoparticles exhibited a comparable lateral size of nickel hydroxide with different lengths of carboxylates which were bidentate coordinated (Figure 1b). The redox reaction was retarded in the case of monolayer nanoparticles with longer alkyl chain length carboxylates owing to the interruption of hydroxyl ion diffusion. The electrochemical catalytic performance for the oxygen evolution reaction was found to be enhanced in the case of a short alkylcarboxylate because of the improved ion diffusion and intrinsic catalytic activity.

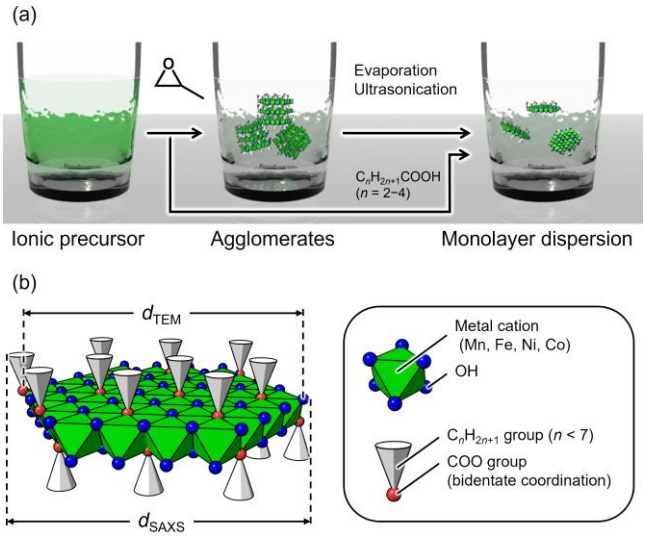

Figure 1. Schematic illustrations of (a) synthesis steps and (b) structure of metal hydroxide carboxylate monolayer nanoparticles. The d_{SAXS} and d_{TEM} shown in (b) are primary particle diameters calculated by using SAXS and TEM, respectively.

NHC nanoparticles were synthesized through previously reported method,[24,26] with modifications. Experimental details are described in Supporting Information. Propylene oxide was added to the ionic precursor solution dissolving nickel chloride and saturated carboxylic acids ($C_nH_{2n+1}COOH$, n = 1–5, 7, 9 and 11). The sample IDs are denoted as NHC-n, where n corresponds to the number of alkyl units of carboxylic acids used. NHC-n (n = 1–5 and 7) formed green colored transparent colloidal dispersions. Although NHC-9 formed a colloidal dispersion, it gradually became a turbid suspension in several minutes. NHC-11 formed an opaque suspension and subsequently precipitated before the vacuum quenching process. These observations indicated the formation of highly aggregated/agglomerated particles when $C_nH_{2n+1}COOH$ had n > 7. Powders were obtained after vacuum evaporation. Figure 2a shows the X-ray diffraction (XRD) patterns of NHC-n (n = 1–5 and 7). All the patterns showed peaks at lower than 2θ = 10°. These peaks indicated the formation of layered structures considering the previous reports.[24,26] Different from the well-crystallized large-sized monolayer The full width at half maximum of the peaks decreased with increasing the number of alkyl chain units (Figure S2). Longer alkyl chain units will show a stronger hydrophobic interaction, which will be a driving force to form a well-ordered layered structure. The lattice spacings are plotted against the alkyl chain unit (Figure 2b). The value increased with different slopes when increasing the number of the alkyl chain unit: the mean increases per alkyl chain unit for n = 1–4 and n = 4–7 were 0.89 Å and 2.11 Å, respectively. Lagaly *et al*. suggested an equation to calculate the tilt angle of the interlayer alkyl anions having monolayer and bilayer arrangements;[29-31] $d_L = d_0 + d_1 + 1.27m\cdot\cos\alpha$ (monolayer) and $d_L = 2d_0 + d_2 + 2.54m\cdot\cos\alpha$ (bilayer), where d_L, d_0, d_1, d_2 and α are lattice spacing, distance between the center of the hydroxide layer and functional head group, distance between the terminal methyl group from the hydroxide layer, distance between the chain ends, and the angle tilting

from the c axis. The α was calculated as 46° for the monolayer arrangement (n = 1–4) and 34° for the bilayer arrangement (n = 4–7). IR spectra were taken to characterize the chemical condition of alkyl carboxylic acids (Figure 2c). IR spectra were normalized by the absorbance of the band of the asymmetric COO stretching vibration ($\nu(COO)_{as}$). The absorbance of bands at 2850–2980 cm^{-1} assigned as $\nu(CH_2)$ and $\nu(CH_3)$ increased relative to $\nu(COO)_{as}$ with increasing n (Figure S3). The wavenumber difference between asymmetric and symmetric COO vibration, $\Delta\nu$ = $\nu(COO)_{as}-\nu(COO)_s$, is known to show the chemical condition of the carboxylic group.[32] The $\Delta\nu$ of NHC-n (n = 1–5 and 7) were comparable to each as approximately 150 cm^{-1}, which was assigned as a bridging bidentate state.

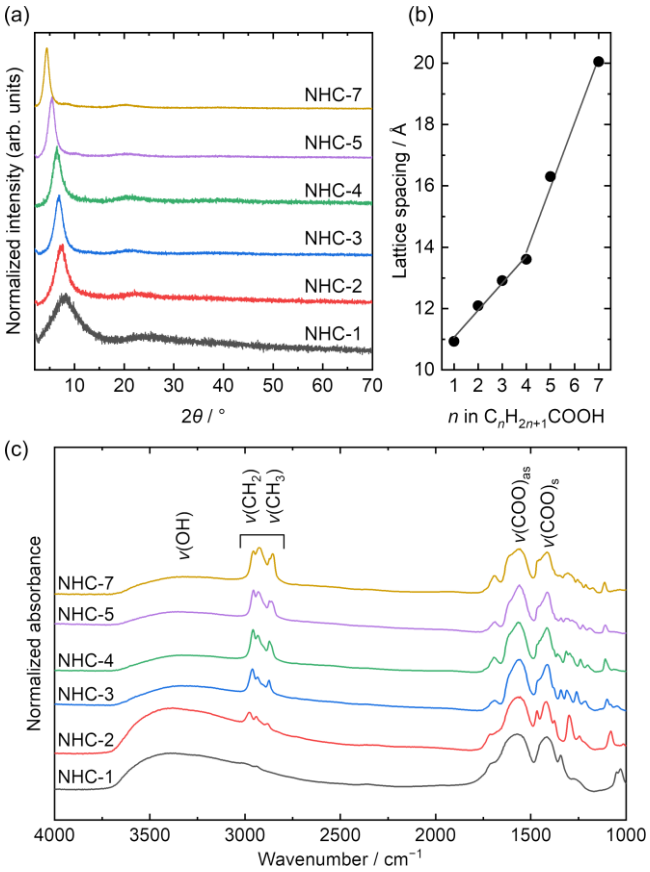

Figure 2. (a) XRD patterns of NHC-n (n = 1–5 and 7) dried powders. (b) Lattice spacing of layered structures with linear fitted data (red solid line). (c) IR spectra of NHC-n (n = 1–5 and 7) dried powders.

The powdery NHC-n (n = 1–5 and 7) were redispersed in ethanol by using ultrasonication with a concentration of 0.5 mol L^{-1} of Ni species. SAXS patterns of the obtained colloidal dispersions and fitted curves using the unified equation proposed by Beaucage and Schaefer[33,34] are shown in Figure 3a. All the patterns showed a drastic intensity decrease in the range of scattering vector > 0.3 nm^{-1}, where Bragg diffraction from layered structures should be observed. This indicates that the layered structures were delaminated by ultrasonication and monolayer nanoparticles were formed. SAXS patterns of NHC-n (n = 1–5) showed a feature of monodispersed nanoparticles. The calculated particle diameters were 1.61, 1.83, 1.96, 2.15 and 2.25 nm for the redispersion of NHC-1, NHC-2, NHC-3, NHC-4 and NHC-5, respectively. However, NHC-7 showed a SAXS pattern well fitted with parameters for two different sized objects. The sizes of the smaller and larger particles were 2.38 nm and 4.65 nm, respectively. TEM observation was employed to observe the nanoscale structure of the synthesized materials. Figure 3b is the TEM image of NHC-7. Individual single-nm-sized particles were observed. The averaged particle diameter was 1.70 nm, therefore, the secondary particles shown in SAXS characterization were assumed as agglomerates. TEM images of redispersed NHC-n (n = 1–5 and 7) were shown in Figure S4. The primary particle diameters calculated by using SAXS (d_{SAXS}) and TEM (d_{TEM}) are summarized in Figure 3b. The d_{SAXS} was found to gradually increase with increasing the number of alkyl units of the carboxylates used. This clearly revealed that the synthesized monolayer nanoparticles were modified by different lengths of carboxylates. However, the d_{TEM} had a comparable value and was irrespective of the number of alkyl units of the carboxylates. Although a TEM grid with a thin carbon deposited membrane support (< 6 nm) was employed, it was hard to observe carboxylate moieties owing to the low electron density contrast compared with the background membrane. As a result, d_{TEM} was assumed to be the diameter of the nickel hydroxide moiety. Considering these observations, the alkyl chain length of carboxylates did not exert a significant effect on the size of the nickel hydroxide moiety. In addition to the above results, the as-synthesized colloidal dispersion of NHC-2, 3 and 4 (just after quenching the reaction by evaporating propylene oxide) was found to show SAXS patterns comparable to the redispersed one as well as calculated diameters (Figure S5). This indicates that NHC monolayer nanoparticles could be directly prepared in the case of NHC-n (n = 2–4).

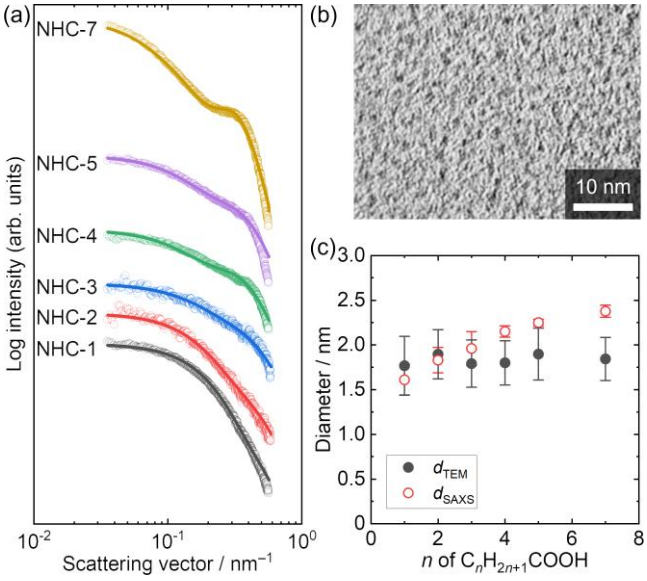

Figure 3. (a) SAXS patterns of redispersed NHC-n (n = 1–5 and 7) colloidal dispersion. (b) TEM image of redispersed NHC-7. (c) Diameters of NHC-n (n = 1–5 and 7) obtained by using TEM (d_{TEM}) and SAXS (d_{SAXS}).

To investigate a chemical compositional versatility of the present synthetic procedure, manganese, iron, and cobalt chlorides and C_2H_5COOH were used to prepare respective nanoparticles. Sample IDs are denoted as MHC-2

(manganese hydroxide propionate), FHC-2(iron hydroxide propionate), and CHC-2(cobalt hydroxide propionate). XRD patterns of MHC-2, FHC-2, and CHC-2 showed broad peaks assigned as layered structures at lower than 2θ = 10° without any peaks (Figure 4a); corresponding lattice spacings were 11.0 Å (MHC-2), 11.1 Å (FHC-2), and 12.0 Å (CHC-2)). IR spectra (Figure S6) showed bidentate coordination of propionate: $\Delta\nu$ of 149 cm^{-1} (MHC-2, bridging), 116−162 cm^{-1} (FHC-2, chelating and bridging), 144 cm^{-1} (CHC-2, bridging). Figure 4b is SAXS patterns of as synthesized colloidal dispersions. All the patterns showed a drastic intensity decrease in the range of scattering vector > 0.3 nm^{-1}, which indicates formation of monolayer nanoparticles same as nickel hydroxide carbonate cases. The calculated d_{SAXS} were 1.72 nm (MHC-2), 2.39 nm (FHC-2), and 1.43 nm (CHC-2). TEM allowed direct observation of monolayer nanoparticles: statistically averaged d_{TEM} were 1.91 nm (MHC-2), 2.19 nm (FHC-2), 1.86 nm (CHC-2) (Figure 4c-4e). Conclusively, the present bottom-up approach to directly synthesize monolayer nanoparticles could be applied to manganese, iron, and cobalt hydroxide carbonates as well as nickel hydroxide carbonate cases.

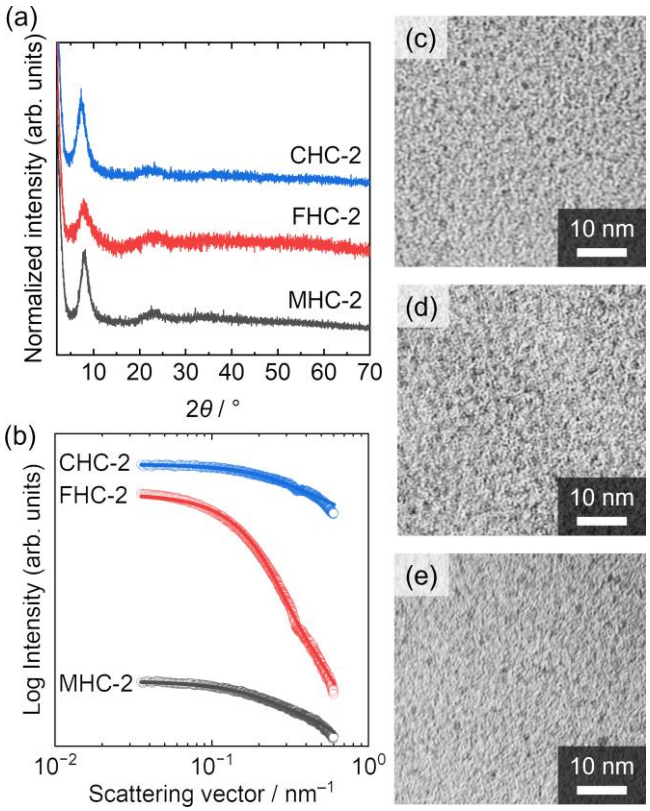

Figure 4. (a) XRD patterns of dried powders and (b) SAXS patterns of as synthesized colloidal dispersions of MHC-2 (black), FHC-2 (red), and CHC-2 (blue), respectively. TEM images of as synthesized (c) MHC-2, (d) FHC-2, and (e) CHC-2.

NHC-2 and NHC-5 were employed to investigate the effect of surface modifier carboxylates on the redox behavior and electrochemical catalytic property. Cyclic voltammetry (CV) curves are shown in Figure 5a and 5b. Both NHC-2 and NHC-5 showed two peaks assigned as the redox reaction of nickel hydroxide;[35]

$$Ni(OH)_2 + OH^- \rightleftarrows NiOOH + H_2O + e^-$$

Redox peak positions of NHC-2 and NHC-5 shifted depending on the scan rate, which indicates the electrochemical reaction was a quasi-reversible process. The redox peak current of NHC-2 was significantly larger than NHC-5. This means that a larger number of Ni sites contributed to the redox reaction. The plot of oxidation peak currents, i_{ox}, and the scan rate, ν, can be fit with a power-law relationship; $i_{ox} = a\nu^b$ (a and b are variables). The b value of NHC-2 and NHC-5 was 0.58 and 0.54, respectively (Figure S6), which indicated a diffusion-controlled redox process.[36,37] Diffusion coefficients were calculated using the classical Randless-Sevcik equation;[38]

$$I_p = 2.69 \times 10^5 m^{3/2} A D_0^{1/2} \nu^{1/2} C_0$$

where I_p, m, A, D_0, ν and C_0 are the peak current, number of electron transferred, electrode area, proton diffusion coefficient, scan rate and concentration of $Ni(OH)_2$ in the solid. C_0 was calculated using the molecular weight of β-$Ni(OH)_2$ and its density of 3.97 g cm^{-3}.[39,40] According to the equation and the slope of I_p-$\nu^{1/2}$ plot shown in Figure 5c, D_o values were calculated. The D_0 of NHC-2 was 1.7×10^{-11} cm^2 s^{-1}, which was 36 times larger than D_o of NHC-5 (4.7×10^{-13} cm^2 s^{-1}). This implied that the steric effect of the larger carboxylate modifiers drastically retarded proton diffusion. Electrochemical impedance spectroscopy (EIS) plots are shown in Figure 5d. The experimental data were well fitted using a reported model circuit composed of solution resistance (R_s), charge transfer resistance (R_{ct}), constant phase elements and Warburg impedance (Z_w).[41] The R_{ct} of NHC-5 was 158 Ω, which is significantly larger than the R_{ct} of NHC-2 (17.9 Ω). Although the particle diameter of $Ni(OH)_2$ will affect the charge transfer resistance,[42] those were comparable for both samples, as shown in Figure 3b. Therefore, the difference in the charge transfer resistance was contributed by the carboxylate moiety. It was assumed that the large distance between conductor and nickel hydroxide monolayer owing to the large-sized carboxylate interrupted electron diffusion and increased R_{ct}. Linear sweep voltammetry (LSV) curves were taken to characterize the electrochemical catalytic performance for an oxygen evolution reaction (Figure 5e). The over potential at a current density of 10 mA cm^{-2} (η_{10}) is one of the criteria for the evaluation of a catalyst. The η_{10} of NHC-2 and NHC-5 was 462 mV and 519 mV. Reported studies suggest that the oxygen evolution reaction proceeds on the surface of a hydroxide involving coordinating ligands.[17,18] The larger diffusion coefficient of NHC-2 may result in a positive effect to lower η_{10}. Here, as is reported by W. Boettcher *et al.*,[43] trace Fe impurity in the electrolyte will lead unexpectedly improvement of electrochemical catalytic performance of Ni-based hydroxides. Fe impurity was not detected in elemental analysis of used KOH solution by X-ray fluorescence spectroscopy and surface elemental analysis of aged NHC-2 and NHC-5 in KOH solution by X-ray photoelectron spectroscopy. These results indicates that the difference of OER performance was derived from difference of coordinating carboxylates. A Tafel plot is shown in Figure 4f. The slopes were 86 mV dec^{-1} for NHC-2 and 105 mV dec^{-1} for NHC-5. This suggested that the intrinsic electrochemical catalytic activity of NHC-2 was superior compared with that of NHC-5.

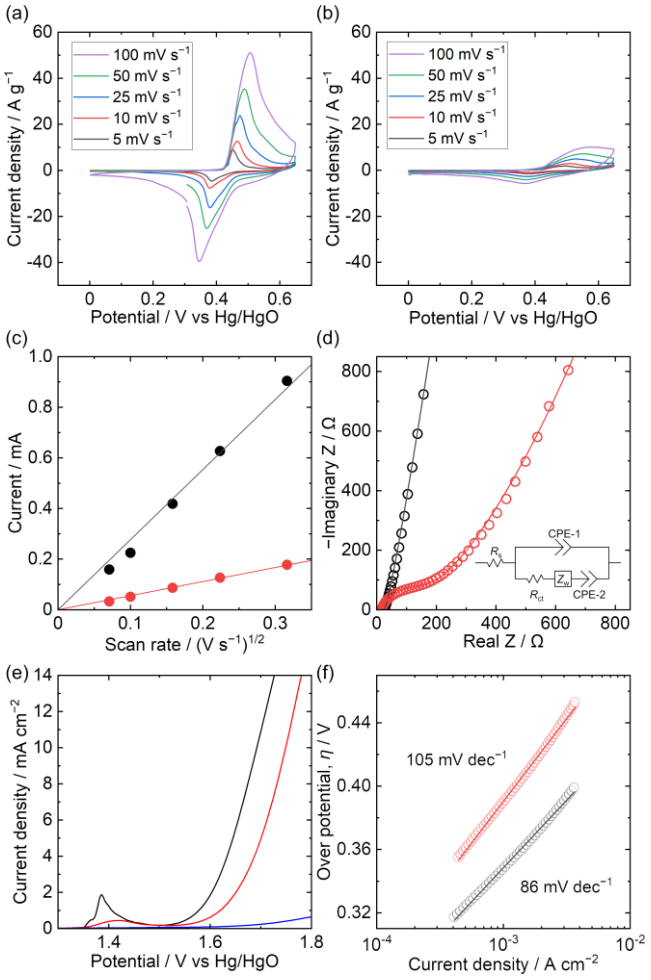

Figure 5. CV curves of (a) NHC-2 and (b) NHC-5 at a scan rate of 5, 10, 25, 50 and 100 mV s^{-1}. (c) Relation between scan rate and oxidation and (d) EIS of NHC-2 (black) and NHC-5 (red) with fitted data (solid line). Inset in panel (d) is an equivalent circuit used for fitting. (e) LSV curves of NHC-2 (black), NHC-5 (red) and pristine carbon electrode (blue). (f) Tafel plot of NHC-2 (black) and NHC-5(red) with corresponding linear fitted data (solid lines).

In summary, metal hydroxide carbonate monolayer nanoparticles were successfully synthesized by an epoxide-mediated alkalinization process with/without ultrasonication. Monolayer nanoparticles were directly formed when carboxylates of $C_nH_{2n+1}COO$ (n = 2–4) were employed. Post treatment of ultrasonication enabled the formation of monolayer nanoparticles having carboxylates of $C_nH_{2n+1}COO$ (n = 1–5). However, monolayer nanoparticles were not formed through the present method when the carboxylate had an alkyl unit number larger than seven. Electrochemical characterization revealed that NHC monolayer nanoparticles with a short length of the alkyl unit showed a larger peak current of the redox reaction and improved electrochemical catalytic performance owing to its high proton diffusion coefficient, lowered electron transfer resistance and improved intrinsic catalytic activity. We propose that the results obtained in this study will provide a novel design strategy of metal hydroxide monolayer nanoparticulate catalysts toward high functionality.

ASSOCIATED CONTENT

Supporting Information.

The Supporting Information is available free of charge via the Internet at http://pubs.acs.org.

Experimental methods; full width half maximum of XRD peaks; IR absorbance area ratio; SAXS patterns; and scan rate dependence of CV peaks (PDF)

AUTHOR INFORMATION

Corresponding Author

Naoki Tarutani – Graduate School of Advanced Science and Engineering, Hiroshima University, Higashi-Hiroshima 739-8527, Japan; CAT Fellow, Institute for Catalysis, Hokkaido University, Sapporo 001-0021, Japan; https://orcid.org/0000-0003-0696-8082;
Email: n-tarutani@hiroshima-u.ac.jp

Author

Sota Kimura – Graduate School of Advanced Science and Engineering, Hiroshima University, Higashi-Hiroshima 739-8527, Japan

Takuya Sakata – Graduate School of Advanced Science and Engineering, Hiroshima University, Higashi-Hiroshima 739-8527, Japan; Western Region Industrial Research Center, Hiroshima Prefectural Technology Research Institute, 2-10-1 Aga-Minami, Kure 737-0004, Japan

Kazumasa Suzuki – Department of Materials Science, The University of Shiga Prefecture, Hikone, Shiga 522-8533, Japan; https://orcid.org/0000-0002-9824-7620

Kiyofumi Katagiri – Graduate School of Advanced Science and Engineering, Hiroshima University, Higashi-Hiroshima 739-8527, Japan; https://orcid.org/0000-0002-9548-9835

Kei Inumaru – Graduate School of Advanced Science and Engineering, Hiroshima University, Higashi-Hiroshima 739-8527, Japan; https://orcid.org/0000-0001-6876-3854

Notes

The authors declare no competing financial interest.

ACKNOWLEDGMENT

This work was supported by JSPS KAKENHI (Grant Numbers JP20K15368, JP21H00149, JP22K14753, and JP22H05143), JSPS Core-to-Core Program, MEXT Leading Initiative for Excellent Young Researchers, MEXT Strategic Professional Development Program for Young Researchers (HIRAKU-Global), the Cooperative Research Program of Institute for Catalysis, Hokkaido University (Grant number 21A1007), the facilities of the Institute of Materials and Systems for Sustainability, Nagoya University, Iketani Science and Technology Foundation, and the Takahashi Industrial and Economic Research Foundation. We thank Edanz (https://jp.edanz.com/ac) for editing a draft of this manuscript.

REFERENCES

(1) Novoselov, K. S.; Mishchenko, A.; Carvalho, A.; Castro Neto, A. H. 2D materials and van der Waals heterostructures. *Science* **2016**, *353*.

(2) Wang, J.; Xu, Y.; Ding, B.; Chang, Z.; Zhang, X.; Yamauchi, Y.; Wu, K. C. W. Confined Self-Assembly in Two-Dimensional Interlayer Space: Monolayered Mesoporous Carbon

Nanosheets with In-Plane Orderly Arranged Mesopores and a Highly Graphitized Framework. *Angew. Chemie Int. Ed.* **2018**, *57*, 2894–2898.

(3) Tan, H.; Tang, J.; Henzie, J.; Li, Y.; Xu, X.; Chen, T.; Wang, Z.; Wang, J.; Ide, Y.; Bando, Y.; Yamauchi, Y. Assembly of Hollow Carbon Nanospheres on Graphene Nanosheets and Creation of Iron–Nitrogen-Doped Porous Carbon for Oxygen Reduction. *ACS Nano* **2018**, *12*, 5674–5683.

(4) Liu, Z.; Song, L.; Zhao, S.; Huang, J.; Ma, L.; Zhang, J.; Lou, J.; Ajayan, P. M. Direct growth of graphene/hexagonal boron nitride stacked layers. *Nano Lett.* **2011**, *11*, 2032–2037.

(5) Shi, Y.; Zhou, W.; Lu, A.-Y.; Fang, W.; Lee, Y.-H.; Hsu, A. L.; Kim, S. M.; Kim, K. K.; Yang, H. Y.; Li, L.-J.; Idrobo, J.-C.; Kong, J. Van der Waals Epitaxy of MoS 2 Layers Using Graphene As Growth Templates. *Nano Lett.* **2012**, *12*, 2784–2791.

(6) Suenaga, K.; Ji, H. G.; Lin, Y.-C.; Vincent, T.; Maruyama, M.; Aji, A. S.; Shiratsuchi, Y.; Ding, D.; Kawahara, K.; Okada, S.; Panchal, V.; Kazakova, O.; Hibino, H.; Suenaga, K.; Ago, H. Surface-Mediated Aligned Growth of Monolayer MoS 2 and In-Plane Heterostructures with Graphene on Sapphire. *ACS Nano* **2018**, *12*, 10032–10044.

(7) Kobayashi, Y.; Yoshida, S.; Maruyama, M.; Mogi, H.; Murase, K.; Maniwa, Y.; Takeuchi, O.; Okada, S.; Shigekawa, H.; Miyata, Y. Continuous Heteroepitaxy of Two-Dimensional Heterostructures Based on Layered Chalcogenides. *ACS Nano* **2019**, *13*, 7527–7535.

(8) Shi, E.; Yuan, B.; Shiring, S. B.; Gao, Y.; Akriti; Guo, Y.; Su, C.; Lai, M.; Yang, P.; Kong, J.; Savoie, B. M.; Yu, Y.; Dou, L. Two-dimensional halide perovskite lateral epitaxial heterostructures. *Nature* **2020**, *580*, 614–620.

(9) Ji, H. G.; Solís-Fernández, P.; Yoshimura, D.; Maruyama, M.; Endo, T.; Miyata, Y.; Okada, S.; Ago, H. Chemically Tuned p- and n-Type WSe2 Monolayers with High Carrier Mobility for Advanced Electronics. *Adv. Mater.* **2019**, *31*, 1–9.

(10) Ago, H.; Okada, S.; Miyata, Y.; Matsuda, K.; Koshino, M.; Ueno, K.; Nagashio, K. Science of 2.5 dimensional materials: paradigm shift of materials science toward future social innovation. *Sci. Technol. Adv. Mater.* **2022**, *23*, 275–299.

(11) Ma, R.; Liu, Z.; Li, L.; Iyi, N.; Sasaki, T. Exfoliating layered double hydroxides in formamide: A method to obtain positively charged nanosheets. *J. Mater. Chem.* **2006**, *16*, 3809–3813.

(12) Miao, J.; Xue, M.; Itoh, H.; Feng, Q. Hydrothermal synthesis of layered hydroxide zinc benzoate compounds and their exfoliation reactions. *J. Mater. Chem.* **2006**, *16*, 474–480.

(13) Hu, L.; Ma, R.; Ozawa, T. C.; Sasaki, T. Exfoliation of layered europium hydroxide into unilamellar nanosheets. *Chem. - An Asian J.* **2010**, *5*, 248–251.

(14) Adachi-Pagano, M.; Forano, C.; Besse, J.-P. Delamination of layered double hydroxides by use of surfactants. *Chem. Commun.* **2000**, 1, 91–92.

(15) Sun, P.; Ma, R.; Bai, X.; Wang, K.; Zhu, H.; Sasaki, T. Single-layer nanosheets with exceptionally high and anisotropic hydroxyl ion conductivity. *Sci. Adv.* **2017**, *3*.

(16) Song, F.; Hu, X. Exfoliation of layered double hydroxides for enhanced oxygen evolution catalysis. *Nat. Commun.* **2014**, *5*, 1–9.

(17) Xiao, H.; Shin, H.; Goddard, W. A. Synergy between Fe and Ni in the optimal performance of (Ni,Fe)OOH catalysts for the oxygen evolution reaction. *Proc. Natl. Acad. Sci. U. S. A.* **2018**, *115*, 5872–5877.

(18) Dionigi, F.; Zeng, Z.; Sinev, I.; Merzdorf, T.; Deshpande, S.; Lopez, M. B.; Kunze, S.; Zegkinoglou, I.; Sarodnik, H.; Fan, D.; Bergmann, A.; Drnec, J.; Araujo, J. F. de; Gliech, M.; Teschner, D.; Zhu, J.; Li, W. X.; Greeley, J.; Roldan Cuenya, B.; Strasser, P. In-situ structure and catalytic mechanism of NiFe and CoFe layered double hydroxides during oxygen evolution. *Nat. Commun.* **2020**, *11*, 1–10.

(19) Zhao, Y.; Zhang, X.; Jia, X.; Waterhouse, G. I. N.; Shi, R.; Zhang, X.; Zhan, F.; Tao, Y.; Wu, L. Z.; Tung, C. H.; O'Hare, D.; Zhang, T. Sub-3 nm Ultrafine Monolayer Layered Double Hydroxide Nanosheets for Electrochemical Water Oxidation. *Adv. Energy Mater.* **2018**, *1703585*, 1–8.

(20) Jia, X.; Zhang, X.; Zhao, J.; Zhao, Y.; Zhao, Y.; Waterhouse, G. I. N.; Shi, R.; Wu, L. Z.; Tung, C. H.; Zhang, T. Ultrafine monolayer Co-containing layered double hydroxide nanosheets for water oxidation. *J. Energy Chem.* **2019**, *34*, 57–63.

(21) Kuroda, Y.; Miyamoto, Y.; Hibino, M.; Yamaguchi, K.; Mizuno, N. Tripodal ligand-stabilized layered double hydroxide nanoparticles with highly exchangeable CO32-. *Chem. Mater.* **2013**, *25*, 2291–2296.

(22) Kuroda, Y.; Koichi, T.; Muramatsu, K.; Yamaguchi, K.; Mizuno, N.; Shimojima, A.; Wada, H.; Kuroda, K. Direct Synthesis of Highly Designable Hybrid Metal Hydroxide Nanosheets by Using Tripodal Ligands as One-Size-Fits-All Modifiers. *Chem. - A Eur. J.* **2017**, *23*, 5023–5032.

(23) Muramatsu, K.; Kamiusuki, Y.; Kuroda, Y.; Wada, H.; Shimojima, A.; Kuroda, K. Direct bottom-up synthesis of size-controlled monodispersed single-layer magnesium hydroxide nanosheets modified with tripodal ligands. *Dalt. Trans.* **2021**, *50*, 3121–3126.

(24) Tarutani, N.; Tokudome, Y.; Jobbágy, M.; Viva, F. A.; Soler-Illia, G. J. A. A.; Takahashi, M. Single-Nanometer-Sized Low-Valence Metal Hydroxide Crystals: Synthesis via Epoxide-Mediated Alkalinization and Assembly toward Functional Mesoporous Materials. *Chem. Mater.* **2016**, *28*, 5606–5610.

(25) Gash, A. E.; Tillotson, T. M.; Satcher, J. H.; Poco, J. F.; Hrubesh, L. W.; Simpson, R. L. Use of Epoxides in the Sol - Gel Synthesis of Porous Iron (III) Oxide Monoliths from Fe (III) Salts. *Chem. Mater.* **2001**, *13*, 999–1007.

(26) Tarutani, N.; Tokudome, Y.; Jobbágy, M.; Soler-Illia, G. J. A. A.; Tang, Q.; Müller, M.; Takahashi, M. Highly Ordered Mesoporous Hydroxide Thin Films through Self-Assembly of Size-Tailored Nanobuilding Blocks: A Theoretical-Experimental Approach. *Chem. Mater.* **2019**, *31*, 322–330.

(27) Tarutani, N.; Tokudome, Y.; Jobbágy, M.; Soler-Illia, G. J. A. A.; Takahashi, M. Mesoporous microspheres of nickel-based layered hydroxides by aerosol-assisted self-assembly using crystalline nano-building blocks. *J. Sol-Gel Sci. Technol.* **2019**, *89*, 216–224.

(28) Tarutani, N.; Katagiri, K.; Inumaru, K.; Ishigaki, T. Size Effect of Hydroxide Nanobuilding Blocks and Nonionic Block Copolymer Templates on the Formation of Ordered Mesoporous Structures. *J. Phys. Chem. B* **2021**, *125*, 4883–4889.

(29) Kopka, H.; Beneke, K.; Lagaly, G. Anionic surfactants between double metal hydroxide layers. *J. Colloid Interface Sci.* **1988**, *123*, 427–436.

(30) Meyn, M.; Beneke, K.; Lagaly, G. Anion-Exchange Reactions of Layered Double Hydroxides. *Inorg. Chem.* **1990**, *29*, 5201–5207.

(31) Meyn, M.; Beneke, K.; Lagaly, G. Anion-Exchange Reactions of Hydroxy Double Salts. *Inorg. Chem.* **1993**, *32*, 1209–1215.

(32) Nakamoto, K. *Infrared and Raman Spectra of Inorganic and Coordination Compounds*; John Wiley & Sons, Inc.: Hoboken, NJ, USA, 2008.

(33) Beaucage, G.; Schaefer, D. W. Structural studies of complex systems using small-angle scattering: a unified Guinier/power-law approach. *J. Non. Cryst. Solids* **1994**, *172–174*, 797–805.

(34) Beaucage, G. Approximations Leading to a Unified Exponential/Power-Law Approach to Small-Angle Scattering. *J. Appl. Crystallogr.* **1995**, *28*, 717–728.

(35) Oliva, P.; Leonardi, J.; Laurent, J. F.; Delmas, C.; Braconnier, J. J.; Figlarz, M.; Fievet, F.; Guibert, A. de. Review of the structure and the electrochemistry of nickel hydroxides and oxy-hydroxides. *J. Power Sources* **1982**, *8*, 229–255.

(36) Wang, J.; Polleux, J.; Lim, J.; Dunn, B. Pseudocapacitive Contributions to Electrochemical Energy Storage in TiO 2 (Anatase) Nanoparticles. *J. Phys. Chem. C* **2007**, *111*, 14925–14931.

(37) Brezesinski, T.; Wang, J.; Tolbert, S. H.; Dunn, B. Ordered mesoporous α-MoO3 with iso-oriented nanocrystalline walls for thin-film pseudocapacitors. *Nat. Mater.* **2010**, *9*, 146–151.

(38) Pletcher, D.; Greff, R.; Peat, R.; Peter, L. M.; Robinson, J. Potential sweep techniques and cyclic voltammetry. In *Instrumental Methods in Electrochemistry*; Elsevier, 2010; pp 178–228.
(39) Wang, X. Y.; Yan, J.; Zhang, Y. S.; Yuan, H. T.; Song, D. Y. Cyclic voltammetric studies of pasted nickel hydroxide electrode microencapsulated by cobalt. *J. Appl. Electrochem.* **1998**, *28*, 1377–1382.
(40) Oshitani, M.; Takayama, T.; Takashima, K.; Tsuji, S. A study on the swelling of a sintered nickel hydroxide electrode. *J. Appl. Electrochem.* **1986**, *16*, 403–412.
(41) Tarutani, N.; Tokudome, Y.; Jobbágy, M.; Soler-Illia, G. J. A. A.; Takahashi, M. Microparticles with hetero-nanointerfaces: controlled assembly of cobalt hydroxide and nickel hydroxide nanoclusters towards improved electrochemical functions. *J. Mater. Chem. A* **2019**, *7*, 25290–25296.
(42) Wang, R.; Lang, J.; Liu, Y.; Lin, Z.; Yan, X. Ultra-small, size-controlled Ni(OH)2 nanoparticles: Elucidating the relationship between particle size and electrochemical performance for advanced energy storage devices. *NPG Asia Mater.* **2015**, *7*, e183-7.
(43) Trotochaud, L.; Young, S. L.; Ranney, J. K.; Boettcher, S. W. Nickel-Iron oxyhydroxide oxygen-evolution electrocatalysts: The role of intentional and incidental iron incorporation. *J. Am. Chem. Soc.* **2014**, *136*, 6744–6753.

Table of Contents